VI International Conference on Computational Bioengineering
ICCB 2015
M.Cerrolaza and S.Oller(Eds)

VARIANCE-REDUCED SIMULATION OF STOCHASTIC INDIVIDUAL-BASED MODELS FOR TUMOR GROWTH

A. LEJON* AND G. SAMAEY*

* Department Computer Science
KU Leuven
Celestijnenlaan 200A, 3001 Leuven, Belgium
email: firstname.lastname@cs.kuleuven.be

Key words: **Variance Reduction** **Multiscale Model** **Tumor Growth**

1 INTRODUCTION

Tumor growth is a complex biological phenomenon consisting of processes on different scales. On the cellular level – which will be referred to as the microscopic scale – one has to track the random motion of cells, as well as the cell division and cell death. The latter are governed by numerous intracellular processes. Furthermore, the cellular behavior is strongly coupled to the environment and vice versa. For example, cell proliferation is determined by the local oxygen concentration and the local cell density while hypoxia on the other hand can trigger apoptosis, but cells also consume oxygen. This two-way feedback creates a very specific dynamics characterizing the development of the tumor. A hypoxic zone develops in the middle of the tumor, which in turn triggers endothelial cells to vascularize the tumor. This process, also known as angiogenesis [3], ensures that the tumor's need for oxygen and other nutrients is satisfied, which implies that the tumor can grow further.

Smaller avascular tumors can be easily simulated on the microscopic scale using agent-based models. We can distinguish two classes of models here. On one hand, cellular automata update grid cells based on a number of phenomenological rules [11, 13], while on the other hand lattice-free models typically consist of a set of ordinary differential equations (ODEs) attached to each cell. On long time scales, we are typically interested in the tumor as a whole (macroscopic scale). One can also choose to model the system directly on this scale using continuum models, based on mass balance equations [15, 17, 18, 19]. Despite the fact that this approach is significantly cheaper and easier to analyze than agent-based models, it is not feasible to use it as such since it cannot capture discrete features as branching of a vascular network or events regulated by intracellular concentrations. This insight gave rise to multiscale models where agent-based models are typically used to model the cellular component, while the environment is mostly described by a set of reaction-diffusion PDEs, corresponding to the macroscopic scale. Examples can be found in [1, 8, 14]. For a review about the current state of the art in multiscale-modeling of tumor growth, we refer to [5].

In this paper, we use a multiscale model where the random motion is modeled using stochastic differential equations (SDEs), the intracellular variables for the cell cycle and apoptosis are described by ODEs and the environment, consisting of diffusible components, is modeled by PDEs. The model is a modified version of the cellular automaton model of Owen et al. [14]. The main difference is that the new model is lattice-free.

We propose a novel technique to reduce the variance on the results of the adapted multiscale agent-based model. Due to the random motion and the influence on the environment, the simulations are subject to noise. An agent-based model can be simulated via standard Monte-Carlo algorithms. The noise can be eliminated by increasing the number of particles, at the cost of computational efficiency. Various possible techniques for variance reduction are described in literature, for instance antithetic variables, control variates and importance sampling. Excellent reviews concerning variance reduction algorithms can be found in [2].

In this paper, a control process will be introduced for variance reduction. The control process contains all details of the microscopic model except for cell births, cell deaths and VEGF se-

cretion. The key point is to couple the simulation of the macroscopic model with this control process.
We first give a detailed overview of the different layers of the model in Section 2. This model is similar to the model used to describe bacterial chemotaxis [16], and reproduces the features of the cellular automaton model proposed by Owen *et al.* [14]. We describe the variance reduction algorithm in Section 3, and we illustrate the technique numerically in Section 4. Finally, the conclusions are listed in section 5 and we elaborate on a few possibilities for future research.

2 MODEL

In this section, we describe a multiscale model for tumor growth. The microscopic model for tumor growth is based on the ideas used to describe bacterial chemotaxis [6, 16], but our goal was to develop a model that could reproduce the features from the cellular automaton model proposed by Owen et al.[14] and reduce the variance on the resulting densities.
We distinguish two main components: the environment, modeled by a couple of reaction diffusion equations and the agent-based model describing the individual cellular motion and internal variables (e.g. cell cycle, apoptosis state and internal VEGF concentration) attached to each cell.
We consider three types of cells, indexed by $1 \leq p \leq P = 3$: normal cells ($p = 1$), cancer cells ($p = 2$), and endothelial cells (that build up blood vessels, $p = 3$). For each of these cell types, we consider an ensemble of $I_p(t)$ cells, and consider three state variables: position $x \in \mathbb{R}^2$, cell cycle phase $\phi \in [0,1]$ and internal state $z \in \mathbb{R}^{d_p}$, where d_p denotes the dimension of the internal state depending on the cell type. These cells evolve according to evolution laws that depend on the concentration $C(x,t)$ of oxygen and $G(x,t)$ of the Vascular Endothelial Growth Factor (which we call the environment).
The advantage of this approach is that our model has a lattice-free cellular component which makes the computational cost only dependent on the number of cells and not on the size of the domain. Remark that the reaction-diffusion PDEs describing the diffusible components of the environment still need to be solved on a grid, but this cost is marginal due to the sparsity of the involved linear systems. This implies that we can easily rescale the system to simulate a larger tumor on a larger domain.
We now give an overview of the notations that will be used throughout the paper, after which we describe the evolution laws for the environment, and detail the evolution laws for each of the cell types. The cell type dependency is mainly caused by cell type dependent coefficients, which will be discussed later on in more detail.

Notation

- The state variables at time t attached to a single cell of type p are position $X_p(t)$, cell cycle phase $\Phi_p(t)$, internal state $Z_p(t)$
- Particle number densities are denoted by $n_p(x,t)$ indexed by a suitable subscript to indicate the nature of the density. To be more specific, $p = 1$ corresponds with normal cells,

while $p = 2$ will be used to denote the cancer cell population and $p = 3$ for endothelial cells. Further, n_v is used to describe the vascular density.

- The evolution of the state variables is influenced in various ways by the (local) environment. The latter will be modelled by means of diffusible components $G(x,t)$ describing the VEGF concentration, while $C(x,t)$ denotes the oxygen concentration.

2.1 Agent-based model

In this section we give a detailed overview of the evolution of the different state variables attached to each cell of the different cellular populations.

Position. The random motion of the position of the cells is described as a biased Brownian motion. Cells of type p move randomly with diffusion coefficient D_p, and the cells are chemotactically attracted towards high concentrations with sensitivity χ_p. This sensitivity is especially important for the endothelial cells, responsible

$$dX_p(t) = \sqrt{2D_p}\mathrm{d}W_t + \chi_p \nabla G(X_p(t)) \left(1 - \frac{n_p(X_p(t),t)}{n_{\max,p}}\right) \delta t. \tag{1}$$

The cell number density n_p, can be computed as:

$$n_p(x,t) = \frac{1}{h_p} \sum_{i=1}^{I_p(t))} K_{h_p}(x - X_{i,p}(t)) \tag{2}$$

where $I_p(t)$ denotes the total number of cells of type p at time t and K_{h_p} denotes a suitable density kernel with bandwidth h_p.[1] Additionally, the system is characterized by non-conservativeness. Both cell division and cell death are obviously crucially important in a growing tumor.

Cell division is modeled by means of the following ODE:

$$\frac{\mathrm{d}\Phi_p(t)}{\mathrm{d}t} = \frac{C(X_p(t),t)}{\tau_{\min,p}(C_{\phi,p} + C(X_p(t),t))} \mathrm{H}\left(\zeta_p(t) - \zeta_{p,\max}\right),$$

where $\tau_{\min,p}$ denotes the minimal time needed for a cell to complete one cell cycle. Remark that $\tau_{\min,p}$ depends on the cell type. To be more specific, cancer cells are able to proceed twice as fast as normal cells during the cell cycle in a given environment (see table 2). Naturally the cell cycle speed depends on the local oxygen concentration $C(X_p(t),t)$ the cell is navigating through while evolving through the cycle. The higher the oxygen concentration, the faster the cycle is completed, while the cell cycle is put on hold when the cell suffers from hypoxia. A more detailed motivation can be found in [14] and its supplementary material.

[1] For the ease of simplicity, we adopted a simple Dirac kernel for the numerical experiment.

Apoptosis. We introduce a sub-cellular module consistent with [14] in order to describe some intracellular concentrations and account for apoptosis:

$$\frac{\mathrm{d}Z_p(t)}{\mathrm{d}t} = F_p(X_p(t), Z_p(t)) \qquad Z_p(t) \in [0,1]^{d_p},$$

where the right hand side depends on the cell type. For the normal tissue, the Z variable contains two components ($d_1 = 2$), namely the p53 concentration $(Z_{p,1}(t))$ and the intracellular VEGF concentration $Z_{p,2}(t)$. The former can be seen as an estimator for the number of mutations that a cell has undergone during its lifetime. We have:

$$\begin{aligned}
\frac{\mathrm{d}Z_{1,p}(t)}{\mathrm{d}t} &= c_1 - c_2 \frac{C(X_p(t),t)}{C_{p53} + C(X_p(t),t)} Z_{1,t,p}, \\
\frac{\mathrm{d}Z_{2,p}(t)}{\mathrm{d}t} &= c_3 - c_4 \frac{Z_{1,p}(t) Z_{2,p}(t)}{J_5 + Z_{2,p}(t)} + c_5 \frac{C(X_p(t),t)}{C_{\mathrm{VEGF}} + C(X_p(t),t)} Z_{2,p}(t).
\end{aligned}$$

Cells are storing VEGF (i.e. $Z_{2,t,p}$) during hypoxic conditions and release it once this intracellular concentration has reached a certain threshold level. Further, $c_1, \dots c_5$ and $C_{\mathrm{p53}}, C_{\mathrm{VEGF}}$ are constants that can be found in table 2. The apoptosis threshold γ_{apt} can then be written as:

$$\gamma_{\mathrm{apt}}(z) = \mathrm{H}\left(z - z_{\mathrm{high}}\mathrm{H}(n_{\mathrm{thr}} - n_1) - z_{\mathrm{low}}\mathrm{H}(n_1 - n_{\mathrm{thr}})\right),$$

where H indicates the Heaviside function. This definition of γ_{apt} implies that normal cells undergo apoptosis if z has reached a certain threshold value depending on the harshness of the environment. The threshold value is lower in case of a harsh environment, defined as $n_1 < n_{\mathrm{thr}}$, where n_{thr} denotes a threshold value for the normal cells. Naturally tumor cells are independent of the p53 since this mechanism to regulate the normal cell cycle doesn't function properly anymore in a tumor. Cancer cells are able to go into a quiescent state when expressed to hypoxic circumstances, meaning that they don't consume any nutrients anymore for a while. However the duration of this quiescent state is limited, which implies that cancer cells will also undergo apoptosis when the hypoxia holds too long. On the other hand, cancer cells have te ability to recover quickly once there is again more oxygen available. This mechanism can be modeled by the following equation:

$$\frac{\mathrm{d}Z_t}{\mathrm{d}t} = \underbrace{A\mathrm{H}(C_{\mathrm{threshold}} - C(X_p(t),t))}_{\text{Linear increase during hypoxia}} - \underbrace{BZ_t\mathrm{H}(C(X_p(t),t) - C_{\mathrm{threshold}})}_{\text{Exponential decay if } C(X_p(t),t) > C_{\mathrm{threshold}}},$$

where A, B are constants. Further, the first term models the hypoxic state, i.e. the local oxygen concentration $C(X_p(t),t)$ drops below the threshold level $C_{\mathrm{threshold}}$. During this hypoxic period, the internal variable z increases steadily. On the other hand, the second term describes the recovery of the cancer cells if the environment isn't hypoxic anymore, which is captured by the exponential decay term of Z_t. Cancer cells die if $Z_t \geq 1$, corresponding to $\gamma_{\mathrm{apt}}(z) = \delta(z)$, where δ denotes the classical Dirac delta function.

2.2 Coarse Description

An alternative approach to model tumor growth is to describe the evolution of the populations as a whole in a probabilistic way using partial differential equations (PDEs). In general, this approach yields a reaction-diffusion PDE. However, in this case it is not possible to derive a closed formulation for the reaction terms since they all depend on intracellular variables. The macroscopic equivalent of the model without birth and death events can be found in [10], where a continuum description was derived from a agent based stochastic description in different settings:

$$\partial_t n_p(x,t) = D_p \nabla^2 n_p(x,t) - \chi_p \nabla . \left[n_p(x,t) \left(1 - \frac{n_p(x,t))}{n_{p,\max}} \right) \nabla G(x,t) \right], \tag{3}$$

where no reactions (cell divisions, cell deaths) are taken into account. They are consistent in the sense that they satisfy the same evolution equation for the population density in the limit for a large number of particles. Next, we introduce the following macroscopic timestepper: $n_p(x,t^{k+1}) = \mathscr{A} n_p(x,t^k)$, which uses a first order forward Euler discretization to discretize the time derivative and a second order central finite volume scheme to discretize the spatial derivatives. Further details can be found in section 4.

2.3 Environment

The cellular environment consists of two diffusible components regulating the behavior of the cells in various ways. Oxygen denoted by C, is evidently important for the cells to proceed through the cell cycle. The local oxygen concentration is determined from the following equation:

$$\partial_t C(x,t) - \underbrace{D_C \nabla^2 C(x,t)}_{\text{diffusion}} - \underbrace{\psi_C n_v(x,t)(C_{\text{blood}} - C(x,t))}_{\text{exchange with blood}} + \underbrace{C(x,t) \sum_{p=1}^{P} k_{C,p} n_p(x,t)}_{\text{Consumption}} = 0, \tag{4}$$

where D_C is the diffusion coefficient, ψ_C denotes the permeability of the oxygen through the vessels. Next, $n_v(x,t)$ describes the surface area occupied by the vessel at position x and it is defined as $2\pi L(x,t)R(x,t)$, where $L(x,t)$ and $R(x,t)$ respectively denote the length and radius of the vessel segment corresponding with the vessel surface area per unit tissue volume. Further, $C_{\text{blood}}(x,t)$ defines the oxygen concentration in a blood vessel located at position x. The last term in (4) reflects the fact that all cell types consume oxygen with a cell specific rate $k_{C,p}$ and hence it is evident that there is a proportionality to the population density n_p, defined in (2).

3 VARIANCE REDUCTION

In this section we propose a variance reduction algorithm for the tumor model described in section 2. A straightforward agent-based simulation can deliver all the details concerning cell divisions, cell deaths and VEGF secretion, which are obviously crucially important for the

development of the tumor. However this approach is not suitable as such since the results are greatly influenced by the noise originating from the random cellular motion. This noise can reduced by antithetic variables, control variates and importance sampling but only at the expense of extra computational cost. Here, we propose a variance reduction technique using a *control process*.

Control process The *control* cells move in the same way as the real population cells, meaning that they perform the same random jumps as their corresponding realistic counterpart. However they can't divide or die. Nor, they can't secrete VEGF to their environment.

$$dX_p^c(t) = \sqrt{2D_p}\mathrm{d}W_t^c + \chi_p \nabla G(X_p^c(t),t),$$

and analogous to the real system the cell number density – denoted by n^c – can be calculated as:

$$n_p^c(x,t) = \frac{1}{h_p}\sum_{i=1}^{I_p(t)} K_{h_p}(x - X_{i,p}^c(t)),$$

The fact that this system is conservative implies that it is perfectly possible to derive an evolution equation in the macroscopic limit and hence the evolution of this *control* process can be calculated in both a stochastic and a deterministic way (see equations (1), (3). The resulting densities will be denoted by n_p^c and $\tilde{n}_p^c$ respectively.

An improved estimator First notice that the behavior of the real cells can be described as the superposition of a drifted Brownian motion and reactions. Since the first part is completely equivalent to the control process, it is possible to split the population density n_p as:

$$n_p(x,t) = n_p^c(x,t) + R_p(x,t), \tag{5}$$

where $R_p(xt)$ denotes the reaction term during the time-step and it is defined as:

$$R_p(x,t) = \frac{1}{h}\sum_{i=1}^{I_p(\delta t)} \underbrace{K_{h_p}(x - X_{i,p}(t))\,\mathrm{H}(\Phi_{i,p}(t) - 1)}_{\text{Cell divisions}} - \underbrace{K_{h_p}(x - X_{i,p}(t))\,(\delta(\gamma_{\text{apt}}(Z_{i,p}(t)))}_{\text{Apoptosis}}. \tag{6}$$

We propose to construct a variance-reduced estimator based on the deterministic equivalent of n_c^p:

$$\bar{n}_p(x,t) = \tilde{n}_p^c(x,t) + R_p(x,t)$$

Algorithm 1. *The resulting algorithm reads as follows:*

- *Initialize the different cell populations with the corresponding number of agents $I_p(0)$. Furthermore, we also initialize the equivalent coarse description such that the cell number densities are the same: $\tilde{n}(x,0) = n(x,0)$, where $\tilde{n}$ denotes the coarse density.*

- *Next, perform one time-step with the macroscopic simulation, resulting in* $\tilde{n}_p(x,\delta t)$.
- *In parallel, each of the cells are also simulated over a time-step, which yields the corresponding cell number densities* $n_p(x,\delta t)$ *where the cell divisions, apoptosis and VEGF secretion events are taken into account.*
- *The improved estimate for the cell number densities will be denoted by* $\bar{n}_p(x,\delta t)$ *and can be derived as:*

$$\bar{n}_p(x,\delta t) = \tilde{n}_p(x,\delta t) + R_p(x,\delta t), \tag{7}$$

This procedure will be repeated after reinitializing the control density $\tilde{n}_p(x,t) = \bar{n}(x,t)$. The importance of reinitialization can be illustrated by looking into the following hypothetical situation. Suppose the ith cell of type p divides at time $t = t^\star$, and hence cell $I_p + 1$ is born. At time $t > t^\star$, this newborn cell has moved randomly through the domain. Apart from this random motion, it also has influenced the environment along its track. Those events cannot be taken into account without reinitialization.

4 NUMERICAL EXPERIMENTS

In this section, we will illustrate the performance of the variance algorithm described above with a numerical experiment. The cells are living on a 50×50 square grid. The cancer cells are initially uniformly distributed on the square $[1.2 \times 10^{-3}, 2 \times 10^{-3}]^2$ in the middle of the domain, while the normal tissue is uniformly distributed over the whole domain.
Further, we initialize the environment as follows: two straight vessels at $x = 20\Delta x$ and $x = 40\Delta x$, corresponding to a moderate vascular density of $50\text{cm}^2/\text{cm}^3$ (see [14]). The latter results in average oxygen concentrations, meaning that cells are proceeding through the cell cycle at a speed which is slightly higher than half maximal. More details concerning realistic vascular densities and oxygen concentrations can be found in the supplementary material provided with [14].
In the first experiment, we assume a normal tissue containing 2500 cells and a small tumor of 200 cells (weighted with a factor 0.25). The domain is discretized with a gridspace of $\Delta x = \Delta y = 4 \times 10^{-3}$cm. We perform 2000 timesteps with a timestep $\delta t = 1800$s, which is consistent with [14]. Since we are investigating the hypothetical situation of a static vasculature, cell death for cancer cells has been switched off. Otherwise, all cells would die because of the hypoxic environment.

Evolution of populations In figure 1 we show the evolution of normal and cancer tissue, along with the oxygen concentration at time $t = 1.8 \times 10^4$s One can observe that the tumor immediately influences the normal tissue in the sense that most of normal cells die in this cancerous region. In the meantime tumor starts to grow along the vessel until the tissue is locally saturated, meaning that $\sum_{p=1}^{P} n_p(x,t) > n_{p,\max}$. The high birth rate can be explained by the high oxygen concentration. Besides, the cells also diffuse in the other directions due to the random Brownian motion. This evolution can also be seen as an illustration of the "go or grow"-theorem, which is identified as an important characteristic of the aggressiveness of the

tumor [7, 9].
The results shown after 2000 timesteps are shown in the second row of figure 1. The tumor made a hole in the normal tissue while the cancer cells divided along the second vessel, which makes the correlation with the oxygen concentration –shown in the third column– clear. Eventually, almost the the whole normal tissue died in favor of the tumor, while the tissue is fully saturated along the vessels.

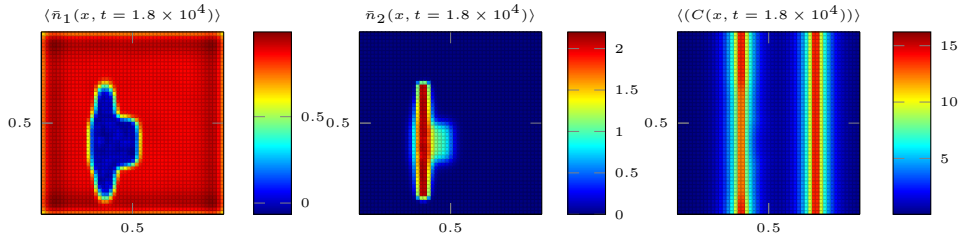

Figure 1: Evolution of mean cellular densities (normal tissue:left, cancer cell density: middle panel) and mean oxygen concentration (right) calculated using variance reduction. In the figure the results at $t = 1.8 \times 10^4$s) are shown)

Evolution of the variance. In figure 2, we compare the variance on the mean cancer cell density with ($\bar{n}_2$) and without n_2 variance reduction at several time slots. In the beginning, cells only divide along the leftmost vessel until the environment is locally saturated (see also figure 1) after which the locations of new divisions move along the vessel. The latter is directly correlated to the peaks in the variance. At time $t = 3.6 \times 10^6$s, the maximal density along the vessels has been reached and hence the peaks are eliminated. Without variance reduction, the variance is lower but not negligible, because of the noise due to random motion. In contrast, after applying variance reduction the variance is significantly lower along both vessels. Remark that the variance is slightly higher next too the vessel. This phenomenon can be explained since there is still enough space for cells to divide here. The asymmetry between the left and the right vessel is due to the initial condition. To be more specific the tumor was initially placed near the leftmost vessel, implying that there are no birth events here because of the volume restriction.

5 CONCLUSIONS AND OUTLOOK

We developed a novel variance reduction technique specifically suited to reduce the noise of agent-based models with birth and death events, as it is the case in our model for tumor growth. We proved that the algorithm outlined in section 3 gave rise to an unbiased estimator and the variance is determined by the births and deaths. The performance was illustrated numerically and the evolution and we analyzed the evolution of the variance on the mean cancer cell density. The proposed algorithm is based on the idea of control variates, since the evolution of the system without reactions is known deterministically via the macroscopic equation (3). A valuable extension would be to combine this algorithm with other variance reduction techniques such

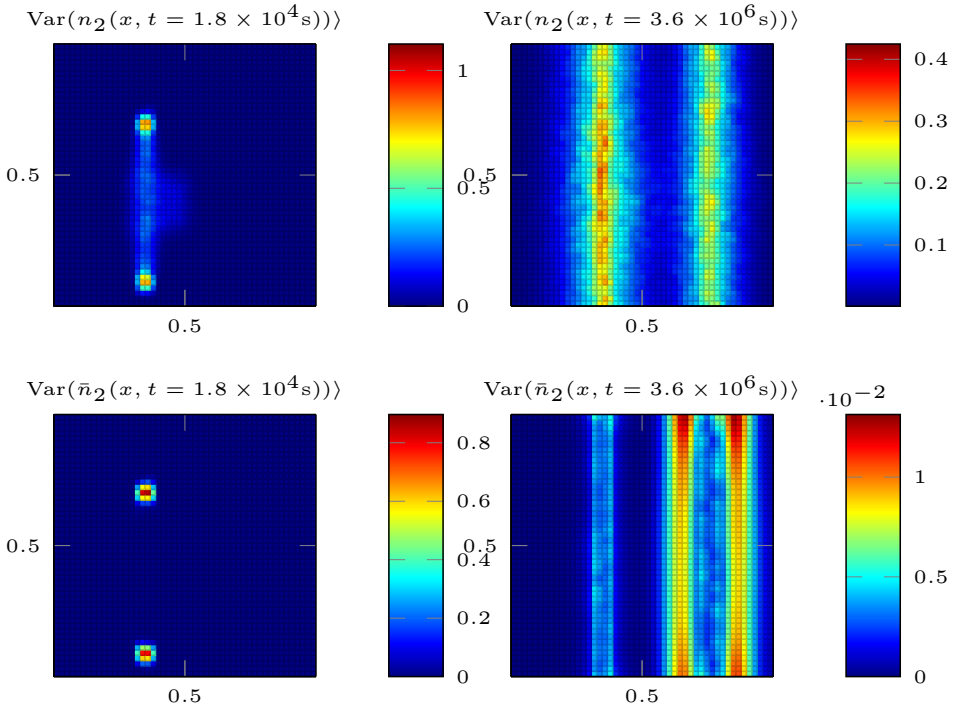

Figure 2: Evolution of variance on mean cancer cell density with (second row, corresponding to $\mathrm{Var}(\langle \bar{n}_2 \rangle)$) and without variance reduction (first row, corresponding to $\mathrm{Var}(\langle n_2 \rangle)$)

as importance sampling. Further, it also would be interesting to test the performance in more realistic cases where the vasculature is developing according to the needs of the tumor. The evolution of the vascular network will have implications on the diffusible fields and therefore on the behavior of the different cell populations. Apart from that, we will also extend our model with important features such as haptotaxis in response to the extra-cellular matrix and include a more sophisticated model for stemcellness [4, 12] since it was identified as one of the hallmarks of cancer [8].

Parameter	Oxygen	units
D	2.4167×10^{-5}	cm^2/s
ψ	0.1	cm/s
δ	0	s^{-1}
k_{normal}	-0.2167	s^{-1}
k_{cancer}	-0.2167	s^{-1}

Table 1: Parameter values reaction diffusion equations

Parameter	Normal Population	Cancer Population	Endothelial cells	units
D_p	0	8.33×10^{-11}	1.66×10^{-10}	$\mathrm{cm}^2/\mathrm{s}^{-1}$
χ_p	0.0	0.0	3.333×10^{-6}	$\mathrm{cm}^2/\mathrm{s}/\mathrm{nM}$
$n_{p,\max}$	1	1	2	# particles
d	2	1		dimensionless
$\zeta_{p,\max}$	4	∞	4	times
$C_{\phi,p}$	3	1.4		mmHg
$\tau_{p,\min}$	1.8×10^5	9.6×10^4		s
z_{high}	0.8			dimensionless
z_{low}	0.08			dimensionless
n_{thr}	0.75			dimensionless
c_1	3.3333×10^{-5}	3.3333×10^{-5}		s^{-1}
c_2	1.6667×10^{-4}	1.6667×10^{-4}		s^{-1}
c_3	3.3333×10^{-5}	3.3333×10^{-5}		s^{-1}
c_4	3.3333×10^{-5}	3.3333×10^{-5}		s^{-1}
c_5	1.6667×10^{-4}	1.6667×10^{-4}		s^{-1}
A		1		s^{-1}
B		$4.167e-5$		s^{-1}

Table 2: Parameter values related to the populations.

References

[1] Anderson, A. R. a. and Weaver, A. R. a. Tumor morphology and phenotypic evolution driven by selective pressure from the microenvironment. *Cell*, 127(5):905–15, Dec. 2006.

[2] Caflisch, R. E. . Monte carlo and quasi-monte carlo methods. *Acta Numer.*, 7:1–49, 1998.

[3] Carmeliet, P. Angiogenesis in life, disease and medicine. *Nature*, 438(7070):932–936, 2005.

[4] Cicalese, A and Bonizzi, G. The Tumor Suppressor p53 Regulates Polarity of Self-Renewing Divisions in Mammary Stem Cells. *Cell*, 138(6):1083–1095, 2009.

[5] Deisboeck, T.S and Wang, Z. Multiscale cancer modeling. *Annu. Rev. Biomed. Eng.*, 13:127–55, Aug. 2011.

[6] Erban, R. and Othmer, H.G. From Individual to Collective Behavior in Bacterial Chemotaxis. *SIAM J. Appl. Math.*, 65(2):361–391, 2004.

[7] Garay, T. and Juhász, G. Cell migration or cytokinesis and proliferation?–revisiting the "go or grow" hypothesis in cancer cells in vitro. *Exp. Cell Res.*, 319(20):3094–103, Dec. 2013.

[8] Hanahan,D. and Weinberg, R.A. Hallmarks of cancer: the next generation. *Cell*, 144(5):646–74, Mar. 2011.

[9] Hatzikirou, H. and Basanta, D. 'Go or grow': The key to the emergence of invasion in tumour progression? *Math. Med. Biol.*, 29(1):49–65, 2012.

[10] Hillen, T. and Painter, K.J. A user's guide to PDE models for chemotaxis. *J. Math. Biol.*, 58(1-2):183–217, Jan. 2009.

[11] Kavousanakis, M. and Liu, P. Efficient coarse simulation of a growing avascular tumor. *Phys. Rev. E*, 85(3):1–11, Mar. 2012.

[12] Morrison, S.J. and Kimble, J. Asymmetric and symmetric stem-cell divisions in development and cancer. *Nature*, 441(7097):1068–1074, 2006.

[13] Olsen, M. M. and Siegelmann, H. T. . Multiscale Agent-based Model of Tumor Angiogenesis. *Procedia Comput. Sci.*, 18:1016–1025, 2013.

[14] Owen, M. R. and Stamper, I. J.. Mathematical modeling predicts synergistic antitumor effects of combining a macrophage-based, hypoxia-targeted gene therapy with chemotherapy. *Cancer Res.*, 71(8):2826–37, Apr. 2011.

[15] Roose, T. and S. Chapman. Mathematical Models of Avascular Tumor Growth. *SIAM Rev.*, 49(2):179–208, 2007.

[16] Rousset, M. and Samaey, G. Simulating individual-based models of bacterial chemotaxis with asymptotic variance reduction. *Math. Model. Methods Appl. Sci.*, 23(12):2155–2191, 2013.

[17] Spill, F. Guerrero, G. Mesoscopic and continuum modelling of angiogenesis. *J. Math. Biol.*, pages 1–48, 2014.

[18] Stein, A. M. and Demuth,A. M. A mathematical model of glioblastoma tumor spheroid invasion in a three-dimensional in vitro experiment. *Biophys. J.*, 92(1):356–365, 2007.

[19] Wise, S. M. and Lowengrub,J. S. Three-dimensional multispecies nonlinear tumor growth–I Model and numerical method. *J. Theor. Biol.*, 253(3):524–43, Aug. 2008.